Journal of Biomedical Optics

SPIEDigitalLibrary.org/jbo

Molecular imaging of water binding state and diffusion in breast cancer using diffuse optical spectroscopy and diffusion weighted MRI

So Hyun Chung
Hon Yu
Min-Ying Su
Albert E. Cerussi
Bruce J. Tromberg

SPIE

Molecular imaging of water binding state and diffusion in breast cancer using diffuse optical spectroscopy and diffusion weighted MRI

So Hyun Chung,[a] Hon Yu,[b] Min-Ying Su,[b] Albert E. Cerussi,[c] and Bruce J. Tromberg[c]
[a]University of Pennsylvania, Department of Physics and Astronomy, 209 South 33rd Street, Philadelphia, Pennsylvania 19104-6396
[b]University of California, Irvine, Department of Radiological Sciences and Tu & Yuen Center for Functional Onco Imaging, 164 Irvine Hall, Irvine, California 92697
[c]University of California, Irvine, Beckman Laser Institute and Medical Clinic, 1002 Health Sciences Road, Irvine, California 92612

Abstract. Tissue water content and molecular microenvironment can provide important intrinsic contrast for cancer imaging. In this work, we examine the relationship between water optical spectroscopic features related to binding state and magnetic resonance imaging (MRI)-measured water diffusion dynamics. Broadband diffuse optical spectroscopic imaging (DOSI) and MR images were obtained from eight patients with locally-advanced infiltrating ductal carcinomas (tumor size $= 5.5 \pm 3.2$ cm). A DOSI-derived bound water index (BWI) was compared to the apparent diffusion coefficient (ADC) of diffusion weighted (DW) MRI. BWI and ADC were positively correlated ($R = 0.90$, p-value $= 0.003$) and BWI and ADC both decreased as the bulk water content increased ($R = -0.81$ and -0.89, respectively). BWI correlated inversely with tumor size ($R = -0.85$, p-value $= 0.008$). Our results suggest underlying sensitivity differences between BWI and ADC to water in different tissue compartments (e.g., extracellular vs cellular). These data highlight the potential complementary role of DOSI and DW-MRI in providing detailed information on the molecular disposition of water in breast tumors. Because DOSI is a portable technology that can be used at the bedside, BWI may provide a low-cost measure of tissue water properties related to breast cancer biology. [DOI: 10.1117/1.JBO.17.7.071304]

Keywords: bound water; diffuse optical spectroscopic imaging; diffusion weighted magnetic resonance images; breast cancer; extracellular matrix.

Paper 11576SS received Oct. 3, 2011; revised manuscript received Dec. 28, 2011; accepted for publication Jan. 23, 2012; published online Jun. 1, 2012.

1 Introduction

Tissue water provides intrinsic contrast for magnetic resonance imaging (MRI), mammography, and diffuse optical imaging[1–3] and bulk water content increases significantly in cancerous tissues due to increased cellularity and edema.[4–7] Detailed information regarding water mobility and environment can be used to gain further insight into molecular mechanisms of cancer and cancer therapies. The water apparent diffusion coefficient (ADC), obtained using diffusion weighted MRI (DW-MRI), measures the restricted motion of water molecules due to cell membranes and other barriers that inhibit random diffusion of free, unhindered water. An inverse correlation between ADC and cellularity of cancer tissues has been shown,[8–10] and several groups have measured lower ADC values in cancer versus normal or benign tissues.[11,12]

In our previous work, we introduced a bound water index (BWI) calculated from broadband diffuse optical spectroscopy (DOS) data that measures the impact of water association with macromolecules on the ~975 nm near-infrared (NIR) water absorption peak.[6] When water is bound to macromolecules, such as proteins, the water absorption peak at 975 nm undergoes both broadening and red shifting.[13–17] These spectral changes appear as a consequence of variations in the relative contributions of harmonic overtones from fundamental O–H vibrations at 3.05 and 2.87 μm.[17] BWI has been validated in previous studies using DW-MRI, where we observed an inverse correlation between BWI and ADC in homogeneous tissue phantoms.[6] In patient studies, we found significantly greater free water content (i.e., lower BWI) in breast cancer compared to normal tissues, and the amount of free water positively correlated with tumor histopathologic grade.

The use of disk operating systems (DOS)/imaging for breast cancer detection and therapy monitoring has been extensively described using tomography methods[18–23] and handheld probes.[3,6,24–27] In this work, we employed a handheld diffuse optical spectroscopic imaging (DOSI) probe to create broadband (650 to 1010 nm) spectroscopic maps of tissue absorption and scattering with high spectral resolution (<1 nm). In addition to BWI, DOSI spectral content was used to calculate the tissue concentration of hemoglobin (oxy-, deoxy-, and total), lipid and water. We measured eight infiltrating ductal carcinoma (IDC) patients with DW-MRI and DOSI in order to investigate the relationship between ADC and BWI in breast cancer. Both indices provide information regarding water environment and disposition that can potentially be useful in breast cancer diagnosis, treatment, and predicting clinical outcome.

Both BWI and ADC values decreased significantly as the bulk water content increased and both showed potential as a prognostic index based on correlations with tumor size. Unlike our previously-reported homogeneous phantom studies, patient measurements of BWI and ADC were positively correlated

Address all correspondence to: So Hyun Chung, University of Pennsylvania, Department of Physics and Astronomy, 209 South 33rd Street, Philadelphia, Pennsylvania 19104-6396. Tel: +215-898-6833; Fax: +215-573-6391; E-mail: sophiechung12@gmail.com.

0091-3286/2012/$25.00 © 2012 SPIE

($R = 0.90$, p-value $= 0.003$), potentially highlighting the importance of microscopic-scale barriers to diffusion encountered *in vivo*. Based on the results of this study and related literature, we hypothesize that BWI is weighted toward water averaged over a large volume with significant contributions from "unbound" water in the extracellular matrix, while ADC primarily reflects the impact of well-defined barriers to diffusion in small volumes such as cells and heterogeneous extracellular compartments. Overall, this work demonstrates the complementary role of DOSI and DW-MRI in providing detailed information on the molecular disposition of water in breast cancer, and suggests that these measurements can be useful in understanding mechanisms of cancer appearance and therapy response.

2 Methods

2.1 *Subjects*

This clinical study was reviewed and approved by the Institutional Review Board of University of California, Irvine, and informed consent was obtained from all human subjects. Eight IDC patients were measured with both DOSI and DW-MRI prior to the initiation of any form of therapy. The maximum tumor dimension of the patients was 5.5 ± 3.2 cm and the age distribution was 44.0 ± 12.3 with a range of 28 to 65.

2.2 *Broadband DOSI Measurements*

Details of the DOSI system have been previously reported.[6,25,28–30] Briefly, DOSI combines broadband frequency domain photon migration (FDPM) using six diode lasers with broadband steady state (SS) spectroscopy in the wavelength range of 650 to 1010 nm. The frequency-dependent (50 to 400 MHz) amplitude and phase of diffusely reflected, temporally-modulated photon density waves are measured and compared to photon diffusion models for each diode laser. Model fits yield absorption, μ_a, and reduced scattering, μ_s', coefficients for large subsurface tissue volumes, typically $\sim$10 cm^3 for our breast probe with a 2.9 cm source-detector separation. Broadband scattering and absorption spectra are calculated by combining FDPM source data with SS diffuse reflectance and imposing a Mie scattering constraint on the wavelength-dependence of scattering. Extinction coefficient spectra of major NIR absorbing components of tissue (oxy-hemoglobin, deoxy-hemoglobin, water, and lipid) are fit to the tissue absorption spectrum in order to calculate concentration.

The BWI is determined from the residual between the normalized tissue water spectrum and a pure water spectrum as described in Chung et al.[6] Figure 1 (reprinted from Ref. 6), demonstrates how the BWI was calculated using the tissue spectra. Briefly, the tissue water spectrum was obtained by subtracting contributions of the other major physiological components (oxy- and deoxy-hemoglobin, and lipid) from a tissue absorption spectrum. Then the residual between the water-only tissue absorption spectrum and a pure water spectrum was calculated by subtracting the pure water spectrum from the normalized tissue water spectrum in the water peak range. The residual is represented as an index, BWI, by averaging the difference between 935 and 998 nm as shown below:

$$\mathrm{BWI} = \frac{\sum_i \left| \frac{\mu_{a,\text{tissue water}}(\lambda_i)}{\mathrm{ctH_2O}} - \mu_{a,\text{pure water}}(\lambda_i) \right|}{N} \times 1000, \qquad (1)$$

where λ_i is ith wavelength (935 nm $\leq \lambda_i \leq$ 998 nm), $\mathrm{ctH_2O}$ is the fraction of measured tissue water divided by pure water concentration (55.6 M) (24), and N is the number of wavelength points in the sum (6). In our previous study with 18 subjects, the BWI of the malignant and normal breast tissues was in the range of 1.96 ± 0.3 and 2.77 ± 0.4, respectively.

DOSI measurements were performed by scanning a hand-held probe on lesion containing and contralateral normal breasts in a grid pattern with 1 cm increments. The range of the scan covered the entire lesion, including surrounding tissue, determined by palpation, ultrasound, mammography or MRI. Details of DOSI patient line- and grid-scanning measurements have been described.[6,25,30] Grid images of oxy- and deoxy-hemoglobin, water, and BWI were generated by interpolating the scanned

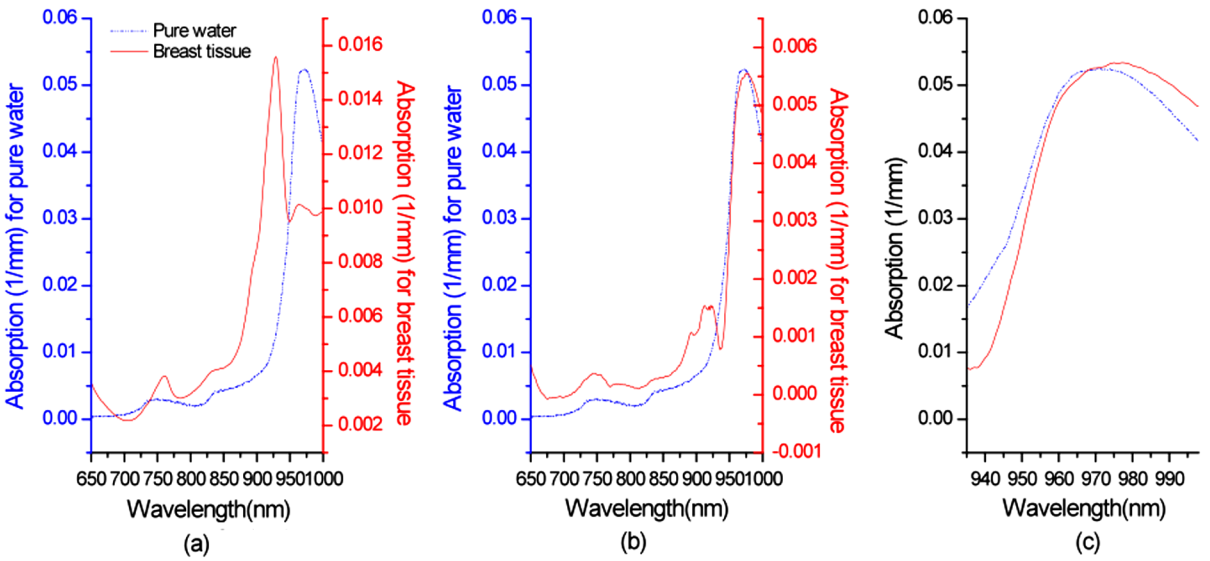

Fig. 1 (a) *In vivo* tissue absorption spectrum (solid line) from normal breast tissue. (b) Tissue water spectrum after subtracting other tissue components' spectra (solid line). (c) Normalized tissue water spectrum at 935 to 998 nm (solid line). The pure water spectrum at 36°C is shown in each panel (a, b, and c, dashed lines) for comparison. [a reprint with permission from IOP publishing, *Phys. Med. Biol.* 53 (2008) 6713–6727, doi:10.1088/0031-9155/53/23/005].

points.[31] In order to compare patient data, an average of BWI values smaller than the threshold determined by the full-width-half-maximum (FWHM) of all the BWI points in an image was calculated and used as a tumor BWI. The BWI point values larger than the threshold in the same image (on the same breast) were used to calculate an average of normal tissue BWI.

DOSI was performed with patients in a supine position. Patients lying in the supine position were able to hold their arms up so that tissue near the chest wall was accessible and the entire lesion could be mapped.

2.3 *MR Measurements for the ADC Acquisition*

All MR images were acquired with a 3.0 T (127 MHz) Philips Achieva scanner using a bilateral 4-channel SENSE (SENSitivity Encoding) breast coil (Philips Medical Systems, Best, The Netherlands). The diffusion-weighted and dynamic-contrast-enhanced images (DCE-MRI) were acquired from a single imaging session in which the DW-MRI is performed prior to the DCE-MRI. The DW-MRI protocol was based on a single-shot spin-echo sequence with echo-planar-imaging acquisition mode using repetition time (TR)/echo time(TE) = 3588/76 ms, field of view(FOV) = 200×200 mm, acquisition-matrix = 128 × 128, pixel size: 1.56 × 1.56 mm, slice thickness: 5 mm, and number of signals averaged = 6. Thirteen sagittal slices of DW image were acquired unilaterally with three b factors (b = 333, 667, and 1000 s/mm^2) in each of the three orthogonal directions for a generation of a rotationally invariant ADC-map. The acquisition time for DW images was approximately 3.5 min. The DCE-MRI protocol was based on a three-dimensional (3-D) gradient echo sequence using TR/TE = 6.2/1.3 ms, flip-angle = 12-deg, SENSE-factor = 2, and an isotropical voxel size (1 mm^3). The DCE-MRI was acquired in 160 bilateral axial slices using FOV = 32-36 cm and a total of seven dynamic frames with Δt = 98 s. The contrast agent (Ominiscan®, 1 cc/10 lbs) was injected manually at the start of the third frame and then followed by a 10-cc saline flush. In Fig. 2(a), the blue color indicates low enhancement, the yellow color indicates moderate enhancement, and the red color indicates high enhancement in a DCE-MR image. A high-order shimming and a fat suppression based on Philips' SPAIR (Spectral Attenuated Inversion Recovery) technique were utilized in both DW-MRI and DCE-MRI. All MR-images were transferred in DICOM (Digital Imaging and Communications in Medicine) format and post-processed and analyzed off-line using a personal computer.

The lesion was segmented by manually drawing the region of interest (ROI) on the enhancement images [red contour on Fig. 2(a)] generated by subtracting the baseline (mean of the first 2 dynamic frames) from the 4th dynamic frame of the DCE-MRI data. The locations of ROI-voxels were then co-registered onto the sagittal slices of DW images [Fig. 2(b)]. Both the ROI-drawing and co-registration were performed using a program developed using Matlab (The Math Works, Inc., USA). The ADC value was generated for each pixel of the co-registered ROI in sagittal orientation.

The ADC value for each pixel was obtained also using a program developed in-house using Matlab, which performed a least-squares fit to the DW-MRI data according to the following equation:

$$\mathrm{ADC} = \frac{-(\ln S - \ln S_0)}{b}, \tag{2}$$

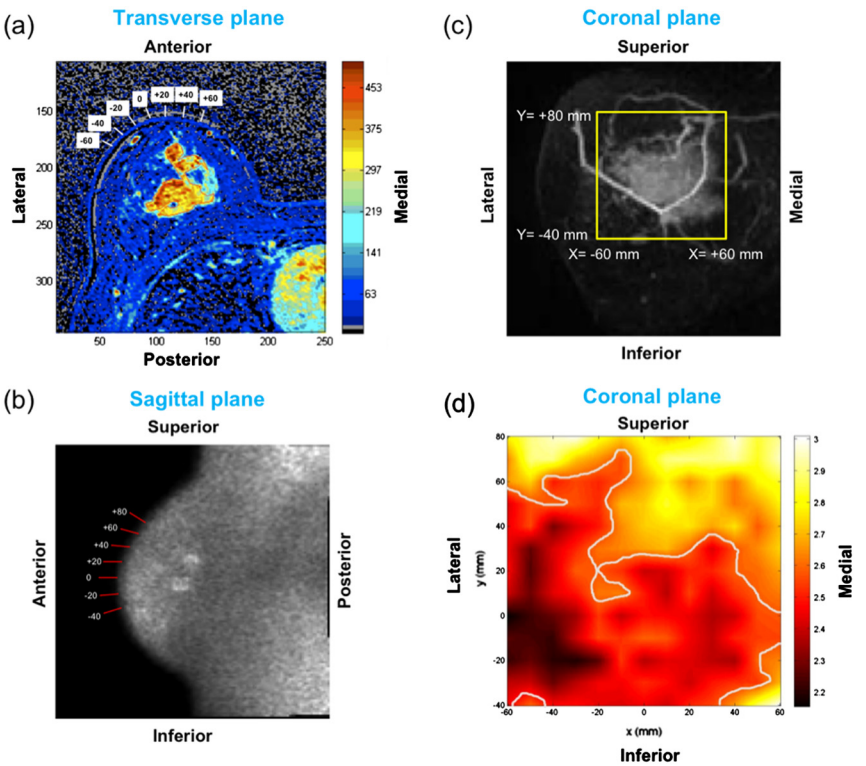

Fig. 2 (a) Transverse dynamic-contrast MR image. The region of interest (red contour) used for ADC calculation and the locations used for lateral scanning of DOSI are shown with white boxes. (b) Sagittal diffusion-weighted-image is shown with the bars indicating where the DOSI probe was positioned axially. (c) Coronal maximum intensity projection image is shown with a yellow box approximating a boundary of the area measured by DOSI. (d) A DOSI acquired BWI image. Darker area with values less than FWHM of the entire points is shown to indicate a tumor area.

where S is the signal intensity measured on the non-zero b factor images ($b = 333$, 667, and 1000 s/mm^2) and S_0 is that of $b = 0$ (no diffusion weighting).

The enhancement images were reformatted to generate a maximum intensity projection image (MIP) in coronal orientation that most closely resembles the two-dimensional presentation of DOSI measurements. [Fig. 2(c)]. All MR images were acquired with the patients in a prone position.

3 Results

Figure 2(a)–2(c) demonstrates DOSI measurement geometry on MR images of a patient. According to the dynamic contrast enhanced images, the tumor size of this patient was $4.9 \times 5 \times 5.5$ cm and was surrounded by very dense breast tissue according to mammography. The Cartesian coordinates of the BWI image on Fig. 2(d) were indicated by the numbers and bars on Fig. 2(a)–2(c). The numbers in the white boxes in Fig. 2(a) show where DOSI probe was positioned laterally, which is the x-axis on the DOSI image shown in Fig. 2(d). The numbers and bars on the diffusion-weighted image [Fig. 2(b)] indicate the axial axis of the DOSI probe positions [the y-axis on Fig. 2(d)]. The tumor area appears brighter in this diffusion-weighted image, which produces lower ADC values than normal fibroglandular tissues according to the equation for ADC calculation (Eq. 2). The yellow box on the MIP image [Fig. 2(c)] approximates the boundary of the points measured by DOSI. Although, Fig. 2(a)–2(c) demonstrates where the DOSI probe was located, the actual tissue volume measured by DOSI is not exactly shown on those MR images because the measurement geometries differed between DW-MRI and DOSI.

ADC values are calculated based on diffusion that occurs within a single $1.56 \times 1.56 \times 5$ mm voxel. ADC values represent an average of many voxels in a given ROI. Most of our tumor data have ADC values below 1.6×10^{-3} mm^2/s, a threshold that differentiated "cancer" from "normal" with 95% sensitivity,[12] while lower than 95% has been used for cancer detection in other studies.[8,11,32,33]

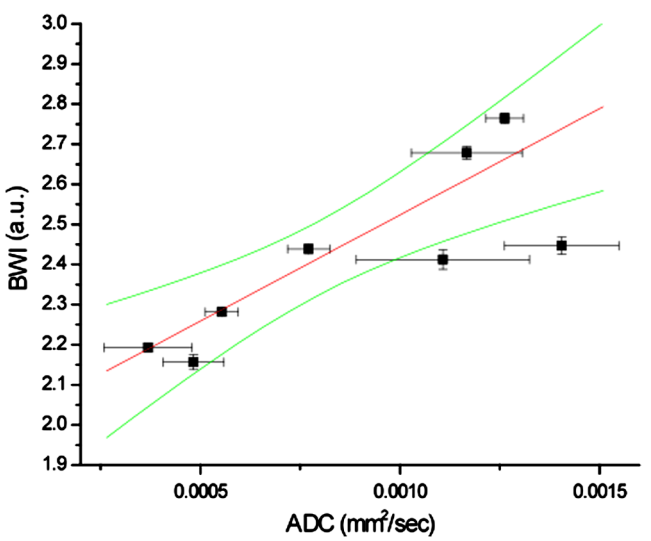

Fig. 3 Correlation between BWI and ADC from *in-vivo* breast cancer measurements of 8 IDC patients ($R = 0.90$, p-value $= 0.003$). 95% confidence interval is shown with green lines. A positive correlation is seen *in vivo*, while negative correlation was previously described in homogeneous tissue phantoms (Ref. 6), suggesting that ADC and BWI are sensitive to water in different tumor compartments.

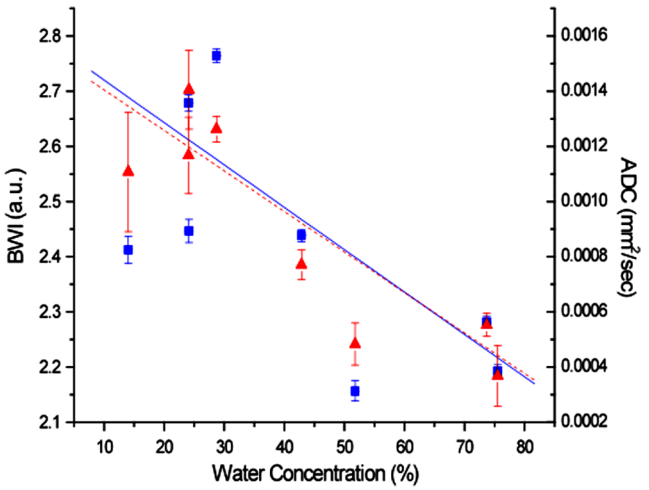

Fig. 4 BWI (squares, solid line) and ADC (triangles, dashed line) vs. Bulk Water Concentration. Both correlate inversely with the bulk water concentration. ($R = -0.81$ and p-value $= 0.016$ for BWI, and $R = -0.89$ and p-value $= 0.003$ for ADC). The bound water fraction and the ADC both decrease as the total tumor water concentration increases.

Figure 2(d) shows a BWI image of the same patient shown in Fig. 2(a)–2(c), measured 8 days after the MRI measurement. The lesion appears as a darker area with lower BWI values than normal tissues as reported in Chung et al.[6]. In this case, BWI $= 2.44 \pm 0.11$ for the darker tumor area and 2.75 ± 0.12 for normal tissues. The smaller BWI values communicate that the high water concentration in cancer tissues contains increased amount of free water rather than bound water.

A relationship between BWI and ADC values measured on the same patients within 6.6 ± 8.1 days is shown in Fig. 3. A positive correlation between the two parameters is observed with $R = 0.9$ and p-value $= 0.003$. The standard errors of BWI are determined from values below the threshold determined by the full-width-at-half-maximum (FWHM) of all BWI values in an image, and from all pixels in an ROI for ADC.

The relationship between DOSI-measured bulk water concentration and BWI and ADC is shown in Fig. 4. Both water parameters significantly decreased with increasing bulk water concentration ($R = -0.81$, p-value $= 0.016$ for BWI and $R = -0.89$, p-value $= 0.003$ for ADC).

Additionally, the relationship between tumor size in maximum dimension and BWI and ADC were examined in Fig. 5. The tumor size is the maximum dimension of the tumor measured by DCE-MRI. BWI and ADC showed comparable inverse correlation with size ($R = -0.85$, p-value $= 0.008$ for BWI and $R = -0.82$, p-value $= 0.013$ for ADC).

4 Discussion

Detailed tissue water property measurements were obtained in breast cancer patients using both optical and MR imaging. The BWI measures the association of water with macromolecules and ADC reflects the mobility of water in a restricted microenvironment. Although, the measurement geometry is different in the two imaging technologies, the same *in-vivo* tumors were measured without compression in order to compare physical and biochemical properties of cancer tissues. Nevertheless, the resolution and field of view are different for DOSI and MRI.

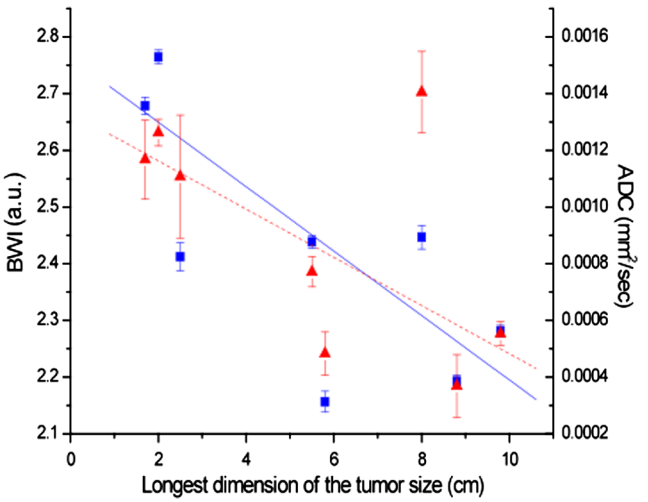

Fig. 5 Relationship between tumor size, BWI and ADC. The water parameters have similar correlation with tumor size, one of the most important prognostic indices of survival ($R = -0.85$ and p-value $= 0.008$ for BWI, and $R = -0.82$ and p-value $= 0.013$ for ADC).

In DOSI, light interrogation over a large (~10 cm^3) tissue volume yields spatially-averaged optical and physiological properties at each probe location. BWI therefore reflects tissue water binding state for all components of cancer tissues: intra- and extracellular spaces as well as vascular structures. In contrast, ADC values are calculated based on diffusion that occurs within a single MRI voxel. Thus, measurements are more heavily weighted toward contributions from cellular diffusion barriers in small volumes in well-defined tumor regions. In contrast, DOSI measurements include contributions from normal tissues and thus represent spatially-averaged macroscopic properties.

These differences in field of view may help explain the positive correlation between BWI and ADC shown in Fig. 3. In our previous work, Ref. 6, BWI was validated in gelatin phantoms by various techniques, including diffusion-weighted MRI. These studies revealed an inverse linear correlation due to the constraining impact of macromolecular binding on water diffusion. Interestingly, the positive relationship between BWI and ADC observed in the current *in vivo* study was the opposite of the correlation measured in homogeneous tissue phantoms. In gelatin, there are no well-defined structural barriers to diffusion comparable to cell membranes or equivalent micro-scale domains. Thus, the positive correlation measured in Fig. 3 is likely a direct result of the heterogeneous, complex, and compartmentalized structure of cancer tissues. It implies that while diffusion becomes more limited due to the presence of small volume barriers, more unbound water is apparent when sampling large tumor volumes. Thus, while all bound water would necessarily have low ADC values, other factors that hinder water mobility likely make contributions to ADC.

The water concentration is known to be high in cancer tissues measured by both MR and optical technologies.[4,6,34–38] The result in Fig. 4 and our previous publication indicate that the high water concentration in cancer tissues contains increased amount of free water rather than bound water. However, interestingly, ADC values decreased (less mobility) as the water concentration increased. This finding also supports that the volumetric difference of tissues used for calculating each water parameter might convey different information regarding the tumor physiology.

There are several important physiologic consequences of this observation. Smaller ADC values have been reported in malignant tumors compared to normal or benign tissues.[8,11,12,39] Restricted diffusion of intracellular water within densely packed, proliferating cancer cells is believed to cause the reduced ADC.[40] The protocol for ADC acquisition and interpretation of the results are actively investigated and has a room for improvement. Nevertheless, the protocol used for ADC measurement in this study is generally considered as a standard that most clinical researchers are utilizing to investigate the application of ADC in differential diagnosis and early therapy response monitoring.[41–46] Many factors may contribute to the measured ADC, including the size of cancer cells, the cell density (or, the relative composition of the cellular and interstitial components), as well as the pseudo-diffusion caused by the microvascular flow (called "intra-voxel incoherent motion [IVIM]"). In this work, we applied three different b-values with the highest $b = 1000$ s/mm^2, so the effect of IVIM is negligible. Thus, cancer tissues with smaller ADC values are likely to have higher cellular density in the ROI.

In the extracellular matrix, hyaluronic acid (HA), a large negatively charged polysaccharide, increases in malignant tumors compared to normal tissues.[6,47] Its polyanionic nature traps water molecules in a mesh structure that exerts swelling pressure.[47] Although, no correlation has been observed between HA content and bound water, HA has been correlated with total volume of water in a study by Sulyok.[48] Thus, it is possible that structured water occupies the space in between HA molecules. Structured water has limited mobility due to the presence of macromolecules and appears in hydration layers outside bound water.[37] Thus, a larger amount of structured vs bound water within the HA extracellular matrix may explain why we observe reduced diffusion but less bound water in cancer tissues. We note that the term "free water" refers to all unbound water including structured water.

High intersitial fluid pressure in cancer tissues due to increased vascular permeability and the absence of a functional lymphatic system may contribute to the increased free water as observed by BWI.[49] Yankeelov et al. also observed a higher volume transfer constant (K_{trans}) due to higher perfusion permeability in an area of rapid proliferation and increased cell density. Their result further supports the measured relationship between ADC and BWI shown in Fig. 3.

In our previous studies, we measured inverse correlations between tumor Nottingham-Bloom-Richardson (NBR) histopathological scores and BWI, and a positive correlation with bulk water content.[6,25] In Figs. 3 and 4, ADC is shown to positively and inversely correlate significantly with BWI and bulk water concentration, respectively. Histopathological scores determine tumor grade, and both grade and size of tumor are the most influential prognostic indices of patient survival.[50] Although, the distribution of NBR scores was not sufficiently broad in this study to examine ADC and BWI correlations, Fig. 5 shows a significant inverse correlation between BWI and maximum tumor dimension, an important index of patient survival. Thus, our current findings, taken together with previous DOSI and MRI studies, provide additional support for BWI as a complementary tumor prognostic index.

In conclusion, the molecular properties of water determined by BWI and ADC appear to reveal different and complementary

aspects of tumor physiology. Although, BWI and ADC are inversely correlated in homogeneous tissue phantoms, they are positively correlated *in vivo*. This suggests that BWI is more sensitive to free water in the extracellular matrix, while ADC reflects contributions from increased tumor cellularity. The relationship between ADC, BWI, and bulk water concentration suggests that both parameters have potential for assessing tumor grade and patient prognosis. This is further supported by measurements linking BWI and ADC with tumor size. Although, BWI and ADC reflect different properties, our results indicate the importance of water as a critical tissue component that can potentially provide unique insight into the molecular patho-physiology of cancer. Their use as molecular imaging endpoints in patients could further advance clinical cancer diagnosis and treatment. It was a limitation of this study that the measured tumors were relatively large (>2 cm). In future studies, we will recruit more patients with small tumors to define patient groups who may receive the most benefit from this complementary information from the two modalities. Lastly, because DOSI is a portable technology that can potentially be used at the bedside, BWI may provide a low-cost measure of tissue water properties.

Acknowledgments

This work was supported by the National Institutes of Health under grants P41-RR01192 (Laser Microbeam and Medical Program: LAMMP), U54-CA105480 (Network for Translational Research in Optical Imaging: NTROI), U54-CA136400, R01-CA142989, NCI-2P30CA62203 (University of California, Irvine Cancer Center Support Grant), NCI-T32CA009054 (University of California, Irvine Institutional Training Grant), Chancellor's Club for Excellence Fellowship of University of California, Irvine, and Susan G. Komen for the Cure Postdoctoral Fellowship. BLI programmatic support from the Beckman Foundation and the Air Force Research Laboratory, under agreement number FA9550-04-1-0101 is acknowledged. The authors wish to thank Montana Compton and Amanda F. Durkin for their assistance as well as the patients who generously volunteered their time for this study. Conflict of interest statement: Bruce J. Tromberg and Albert E. Cerussi report patents, owned by the University of California, related to the technology and analysis methods described in this study. The DOSI instrumentation used in this study was constructed in a university laboratory using federal grant support (NIH). The University of California has licensed DOSI technology and analysis methods to two companies, FirstScan, Inc. and Volighten, Inc. for different fields of use, including breast cancer (FirstScan). This research was completed without participation, knowledge, or financial support of either company, and data were acquired and processed from patients by coauthors unaffiliated with either entity. The IRB and Conflict of Interest Office of the University of California, Irvine, have reviewed both patent and corporate disclosures and did not find any concerns.

References

1. D. J. Manton et al., "Neoadjuvant chemotherapy in breast cancer: early response prediction with quantitative MR imaging and spectroscopy (vol 94, pg 1554, 2006)," *Br. J. Cancer* **94**(10), 1554–1554 (2006).
2. E. A. Sickles, "Breast masses: mammographic evaluation," *Radiology* **173**(2), 297–303 (1989).
3. B. J. Tromberg et al., "Assessing the future of diffuse optical imaging technologies for breast cancer management," *Med. Phys.* **35**(6), 2443–2451 (2008).
4. A. E. Cerussi et al., "In vivo absorption, scattering, and physiologic properties of 58 malignant breast tumors determined by broadband diffuse optical spectroscopy," *J. Biomed. Opt.* **11**(4), 044005 (2006).
5. D. Z. J. Chu et al., "Proton nmr of human-breast tumors—correlation with clinical prognostic parameters," *J. Surg. Oncol.* **36**(1), 1–4 (1987).
6. S. H. Chung et al., "In vivo water state measurements in breast cancer using broadband diffuse optical spectroscopy," *Phys. Med. Biol.* **53**(23), 6713–6727 (2008).
7. L. Spinelli et al., "Bulk optical properties and tissue components in the female breast from multiwavelength time-resolved optical mammography," *J. Biomed. Opt.* **9**(6), 1137–1143 (2004).
8. Y. Guo et al., "Differentiation of clinically benign and malignant breast lesions using diffusion-weighted imaging," *J. Magn. Reson. Imag.* **16**(2), 172–178 (2002).
9. H. Lyng, O. Haraldseth, and E. K. Rofstad, "Measurement of cell density and necrotic fraction in human melanoma xenografts by diffusion weighted magnetic resonance imaging," *Magn. Reson. Med.* **43**(6), 828–836 (2000).
10. Y. Paran et al., "Water diffusion in the different microenvironments of breast cancer," *NMR Biomed.* **17**(4), 170–180 (2004).
11. Y. Kuroki et al., "Diffusion-weighted imaging of breast cancer with the sensitivity encoding technique: analysis of the apparent diffusion coefficient value," *Magn. Reson. Med. Sci.* **3**(2), 79–85 (2004).
12. R. Woodhams et al., "Diffusion-weighted imaging of malignant breast tumors—The usefulness of apparent diffusion coefficient (ADC) value and ADC map for the detection of malignant breast tumors and evaluation of cancer extension," *J. Comput. Assist. Tomo.* **29**(5), 644–649 (2005).
13. L. J. Bellamy, *Advances in Infrared Group Frequencies*, Chapman & Hall, London, pp. 277–288 (1968).
14. S. H. Chung et al., "Non-invasive tissue temperature measurements based on quantitative diffuse optical spectroscopy (DOS) of water," *Phys. Med. Biol.* **55**(13), 3753–3765 (2010).
15. D. Eisenberg and W. Kauzmann, *The Structure and Properties of Water*, Clarendon, Oxford, pp. 8–9, 126–128 (1969).
16. L. Pauling, *The Nature of the Chemical Bond*, Cornell University Press, Ithaca, NY, pp. 449–503 (1960).
17. G. C. Pimentel and A. L. McClellan, *The Hydrogen Bond*, Freeman, San Francisco, pp. 83–85, 225 (1960).
18. R. Choe et al., "Differentiation of benign and malignant breast tumors by in-vivo three-dimensional parallel-plate diffuse optical tomography," *J. Biomed. Opt.* **14**(2), 024020 (2009).
19. S. B. Colak et al., "Clinical optical tomography and NIR spectroscopy for breast cancer detection," *IEEE J. Sel. Top. Quant.* **5**(4), 1143–1158 (1999).
20. G. J. Czarnota et al., "Functional imaging using diffuse optical spectroscopy of neoadjuvant chemotherapy response in women with locally advanced breast cancer," *Clin. Cancer Res.* **16**(9), 2605–2614 (2010).
21. B. W. Pogue et al., "Characterization of hemoglobin, water, and NIR scattering in breast tissue: analysis of intersubject variability and menstrual cycle changes," *J. Biomed. Opt.* **9**(3), 541–552 (2004).
22. B. Pogue et al., "Instrumentation and design of a frequency-domain diffuse optical tomography imager for breast cancer detection," *Opt. Express* **1**(13), 391–403 (1997).
23. P. Taroni et al., "Time-resolved optical mammography between 637 and 985 nm: clinical study on the detection and identification of breast lesions," *Phys. Med. Biol.* **50**(11), 2469–2488 (2005).
24. A. Cerussi et al., "Predicting response to breast cancer neoadjuvant chemotherapy using diffuse optical spectroscopy," *Proc. Natl. Acad. Sci. USA* **104**(10), 4014–4019 (2007).
25. A. Cerussi et al., "In vivo absorption, scattering, and physiologic properties of 58 malignant breast tumors determined by broadband diffuse optical spectroscopy," *J. Biomed. Opt.* **11**(4), 044005 (2006).
26. D. B. Jakubowski et al., "Monitoring neoadjuvant chemotherapy in breast cancer using quantitative diffuse optical spectroscopy: a case study," *J. Biomed. Opt.* **9** (1), 230–238 (2004).
27. B. J. Tromberg et al., "Imaging in breast cancer: diffuse optics in breast cancer: detecting tumors in pre-menopausal women and monitoring

neoadjuvant chemotherapy," *Breast Cancer Res.* **7**(6), 279–285 (2005).
28. F. Bevilacqua et al., "Broadband absorption spectroscopy in turbid media by combined frequency-domain and steady-state methods," *Appl. Opt.* **39**(34), 6498–6507 (2000).
29. D. Jakubowski et al., "Quantitative absorption and scattering spectra in thick tissues using broadbadn diffuse optical spectroscopy," in *Biomedical Optical Imaging*, J. G. Fujimoto and D. L. Farkas, eds., pp. 330–355, Oxford University Press, New York (2009).
30. B. J. Tromberg et al., "Diffuse optical spectroscpy in breast cancer: coregistration with MRI and predicting response to neoadjuvant chemotherapy," in *Translational Multimodality Optical Imaging*, F. S. Azar and X. Intes, eds., pp. 163–183, Artech House, Norwood, MA (2008).
31. W. Tanamai et al., "Diffuse optical spectroscopy measurements of healing in breast tissue after core biopsy: case study," *J. Biomed. Opt.* **14**(1), 014024 (2009).
32. T. Kinoshita et al., "Diffusion-weighted half-Fourier single-shot turbo spin echo imaging in breast tumors: differentiation of invasive ductal carcinoma from fibroadenoma," *J. Comput. Assist. Tomo.* **26**(6), 1042–1046 (2002).
33. R. Woodhams et al., "ADC mapping of benign and malignant breast tumors," *Magn. Reson. Med. Sci.* **4**(1), 35–42 (2005).
34. C. M. Carpenter et al., "Image-guided optical spectroscopy provides molecular-specific information in vivo: MRI-guided spectroscopy of breast cancer hemoglobin, water, and scatterer size," *Opt. Lett.* **32**(8), 933–935 (2007).
35. S. H. Chung et al., "Non-invasive detection and monitoring of tumor pathological grade during neoadjuvant chemotherapy by measuring tissue water state using diffuse optical spectroscopic imaging," *Cancer Res.* **69**(2, Suppl.), 803 (2009).
36. S. H. Chung et al., "Non-invasive measurement of pathological heterogeneity of cancer tissues using water state information from diffuse optical spectroscopic imaging," *Cancer Res.* **69**(24, Suppl.), 5008 (2009).
37. I. Jakobson et al., "MRI of humn tumor exnografts in vivo: proton relaxation times and extracellular tumor volume," *Magn. Reson. Imag.* **13**(5), 693–700 (1995).
38. D. J. Manton et al., "Neoadjuvant chemotherapy in breast cancer: early response prediction with quantitative MR imaging and spectroscopy," *Br. J. Cancer* **94**, 427–435 (2006).
39. S. Sinha et al., "In vivo diffusion-weighted MRI of the breast: potential for lesion characterization," *J. Magn. Reson. Imag.* **15**(6), 693–704 (2002).
40. P. Gibbs et al., "Correlation of ADC and T2 measurements with cell density in prostate cancer at 3.0 Tesla," *Invest. Radiol.* **44**(9), 572–576 (2009).
41. R. Woodhams et al., "ADC mapping of benign and malignant breast tumors," *Magn. Reson. Med. Sci.* **4**(1), 35–42 (2005).
42. E. M. Charles-Edwards and N. M. deSouza, "Diffusion-weighted magnetic resonance imaging and its application to cancer," *Cancer Imaging* **6**(1), 135–143 (2006).
43. A. Matsuoka et al., "Comparison of 3.0- and 1.5-tesla diffusion-weighted imaging in the visibility of breast cancer," *Radiat. Med.* **26**(1), 15–20 (2008).
44. M. Hatakenaka et al., "Apparent diffusion coefficients of breast tumors: clinical application," *Magn. Reson. Med. Sci.* **7**(1), 23–29 (2008).
45. D. A. Bluemke et al., "Diffusion-weighted imaging improves the diagnostic accuracy of conventional 3.0-T breast MR imaging," *Radiology* **256** (1), 64–73 (2010).
46. K. C. Li et al., "The role of parallel diffusion-weighted imaging and apparent diffusion coefficient (ADC) map values for evaluating breast lesions: preliminary results," *Acad. Radiol.* **17**(4), 456–463 (2010).
47. B. P. Toole, "Hyaluronan: from extracellular glue to pericellular cue," *Nat. Rev. Cancer* **4**(7), 528–539 (2004).
48. E. Sulyok, "Physical water compartments: a revised concept of perinatal body water physiology," *Physiol. Res.* **55**(2), 133–138 (2006).
49. S. Ferretti et al., "Patupilone induced vascular disruption in orthotopic rodent tumor models detected by magnetic resonance imaging and interstitial fluid pressure," *Clin. Cancer Res.* **11**(21), 7773–7784 (2005).
50. J. Rosenberg, Y. L. Chia, and S. Plevritis, "The effect of age, race, tumor size, tumor grade, and disease stage on invasive ductal breast cancer survival in the U.S. SEER database," *Breast Cancer Res. Treat.* **89**(1), 47–54 (2005).